International Journal of Greenhouse Gas Control 16 (2013) 167–179

Contents lists available at SciVerse ScienceDirect

International Journal of Greenhouse Gas Control

journal homepage: www.elsevier.com/locate/ijggc

Hydro-dynamically controlled alteration of fractured Portland cements flowed by CO_2-rich brine

L. Luquot*, H. Abdoulghafour, P. Gouze

Laboratoire Géosciences, CNRS, UM2, Place Eugène Bataillon, 34095 Montpellier, France

ARTICLE INFO

Article history:
Received 11 August 2012
Received in revised form 2 April 2013
Accepted 3 April 2013
Available online 29 April 2013

Keywords:
Cement alteration
CO_2 storage
Flow-through experiments

ABSTRACT

Deficient sealing in the well cement plugs and annulus due to mechanical fracturing is an important risk of CO_2 leakage from the reservoir to others permeable layers and the surface. Such situation was reproduced at laboratory scale in order to determine the hydro-chemical control on the fracture permeability. Specifically, we investigated the effect of CO_2 rich-brine flowing through fractured Portland cements at $T = 60\,^{\circ}C$ and $P = 10$ MPa and variable flow rates. We showed that carbonation process is dominant and induces permeability decrease and leakage mitigation for extremely low flow rate whereas for high flow rate injection the permeability remains constant due to the precipitation of a low density secondary Si-rich phase which maintains the initial fracture aperture. At intermediate flow rate the hydraulic aperture can increase due to the densification of the material triggered by the net precipitation of low porosity calcite. These results emphasize that more complex behaviors than those considered from batch experiments may take place in the vicinity of flowing fractures. Specifically, the redissolution of the neoformed calcite as well as the development of amorphous phases, both controlled by the CO_2-rich brine renewing rate in the fracture may prevent the healing fracture.

1. Introduction

Geological carbon storage (GCS) is one of the portfolio solutions for mitigating greenhouse gases emissions (Bachu and Adam, 2003; Hitchon et al., 1999; IPCC, 2005). Substantial progress has been achieved in field of characterization in many types of deep geological formations (such as depleted oil and gas reservoirs or deep saline aquifers) and in the understanding of the interactions between the injected CO_2, the formation fluid and the rock-forming minerals. New models have been developed for various relevant time and space scales, geological and geometrical configurations (e.g. Gunter et al., 2000; Xu et al., 2004). Still, GCS often meets with public opposition mainly due to a negative perception of safety, reliability and controllability of the storage process. Uncompromising questions concern the risk of CO_2 leakage and its negatively impact on human health, valuable resources and environment (Oldenburg et al., 2009). Accordingly, safe, long-term CO_2 geological brings the need for sound approaches to safety assessment and consequently the identification of the risk of leakage from CO_2 storage sites.

Deficient sealing in caprocks due to the presence of fractures is a potential source of CO_2 leakage from the storage reservoir to overlaying layers (Andreani et al., 2008; Ellis et al., 2011) as well as leaky wells which furthermore are potential preferential pathways to the surface. Deficient sealing of wells stems from the mechanical and chemical creation or reactivation of hydraulic discontinuities (fractures) in the cement plugs usually installed before abandonment. Similar risks of sealing deficiency must be envisaged in the cement annulus that is set up after the drilling. The cement annulus ensures both the mechanical stability of the well casing and avoids artificial flow and pressure shortcuts between the reservoir, others permeable layers and ultimately the surface. Both the bulk cement that may be quite heterogeneous because of usual poor control of the emplacement at depth (permeability lower than 10^{-19} m^2) and the cement–caprock and cement–casing interfaces that are mechanically and chemically weak zone (permeability estimated to 10^{-17} m^2 by Crow et al. (2009)) are potential sources of leakage (Celia et al., 2004; Bouc et al., 2009; Carey et al., 2007).

The occurrence of leakage through well-caprocks interface and damaged cements evidently depends on the number of wells (areas with large number of existing, often abandoned, wells, such as: Alberta in Canada and the Texas basin are more exposed) (Celia et al., 2004; Bachu and Watson, 2006) but also on the quality of the well cementation, the history of the well from completion to production activities and past or future geologic events that may alter the initial quality of the sealing (e.g. Bachu and Celia, 2009). Mechanical constraints (deviatoric) are the main sources of irreversible cement damaging. As reported by Deremble et al. (2011), localized mechanical weakness may develop during the well cementing phase and then be enhanced during the pressure

* Corresponding author at: CSIC Barcelona, C/Jordi Girona 18-26, 08034 Barcelona, Spain. Tel.: +34 934006100.
E-mail address: linda.luquot@gm.univ-montp2.fr (L. Luquot).

1750-5836/$ – see front matter © 2013 Elsevier Ltd. All rights reserved.
http://dx.doi.org/10.1016/j.ijggc.2013.04.002

forcing of the reservoir during the CO_2 injection or by tectonic events either natural or initiated by the injection. Whereas these mechanisms of cement damaging are highly probable in the context of CO_2 injection where transient pressure increase takes place, the effects of hydro-chemical processes linked to the presence of CO_2-rich brine and supercritical CO_2 are still insufficiently described for reliable risk assessment purposes.

Very few field observations of cement having been in long contact to CO_2 storage brines are available and none of them concern fractured cements at the origin of CO_2 leakage. Analysis of samples recovered from an abandoned well used for injecting CO_2 during 30 years for EOR display fine thickness of carbonation (50 μm), which appears to clog preexisting micro-fractures inherited from the cement emplacement (Carey et al., 2007). However it is worth noting that these micro-fractures are dead-end discontinuities with no flow, so that mass transfers are driven by diffusion such as in batch experiments. Similarly, Crow et al. (2009) investigated the physicochemical properties of well cement materials subjected to 30 year CO_2 exposure during EOR phase in the Dakota sandstone formation (Utah, USA). They observed local increase of both porosity and permeability in the vicinity of the interface between CO_2-rich fluid and defected cement and casing, due to alteration processes.

Several laboratory investigations of the alteration of cement samples in CO2-rich environments have been published, but finally, there are very few experimental data available to appraise the causal relationships between the presence of fissures in the cement and the occurrence, the rate and the sustainability of CO_2 leaks. Actually, most experimental investigations regarding CO_2 reactivity with Portland-based cements were performed using batch reactor approaches (Jacquemet et al., 2005; Barlet-Gouédard et al., 2006, 2007, 2009; Rimmelé et al., 2008; Duguid et al., 2006; Kutchko et al., 2007, 2009; Liteanu and Spiers, 2010). The advantage of such approach is its simplicity allowing studying a large range of pressure, temperature, geochemical conditions as well as cement composition. Important information concerning the reaction paths and their sensitivity to chemical parameters were acquired. For example, Kutchko et al. (2007), Kutchko et al. (2009) and Sauki and Irawan (2010) investigated the effects of cement curing conditions on the extension of carbonation rate. However, batch experiment cannot reproduce the coupled effects of chemical and hydrodynamical processes, which are controlling the renewing of reactant within the cement matrix due to the flow in the fracture; the main mechanism of transport being diffusion. Consequently it is impossible from batch experiments to quantify the feedback effects of these processes on the permeability of the fracture which is the far most important issue regarding the increase or the mitigation of the leakage rate.

To bridge this gap, experiments reproducing both the thermodynamic and hydrodynamic conditions expected in hydraulically active discontinuities are required. Such experiments in which flow, fluid composition, fracture properties, pressure and temperature are controlled are the only way for modeling the flow, transport and reaction coupled processes and identifying the parameters controlling the time-resolved leakage fluxes (Luquot and Gouze, 2009).

As pointed out by Bachu and Bennion (2009), the core-scale permeability of the undamaged cements bathed in CO_2-rich brine decreases due to the formation of a carbonate ($CaCO_3$) crust triggered by the Portlandite ($Ca(OH)_2$) dissolution:

$$CO_2 + H_2O \leftrightarrow H_2CO_3 \leftrightarrow 2H^+ + {CO_3}^{2-} \quad (1)$$

$$Ca(OH)_2 + 2H^+ + {CO_3}^{2-} \leftrightarrow CaCO_{3(s)} + 2H_2O \quad (2)$$

$$CSH + 2H^+ + {CO_3}^{2-} \leftrightarrow CaCO_{3(s)} + SiO_2OH_x \quad (3)$$

$$CO_2 + H_2O + CaCO_{3(s)} \leftrightarrow Ca^{2+} + 2{HCO_3}^- \quad (4)$$

where CSH denotes calcium silicate hydrate (with Ca/Si ratio of about 1.65) and SiO_2OH_x denotes hydrated silica (silica gel).

Experiments with renewing of the fluid around undamaged cement cores were conducted by Scherer et al. (2005) and Duguid and Scherer (2010). Using a relatively high flow of CO_2-saturated brine through a channel made in a cement sample, Scherer et al. (2005) observed that the protective carbonate layer is continuously re-dissolved and leads to easily observable cement degradation. At the end of the experiment the channel was noticeably enlarged suggesting that the hydraulic conductivity (not measured by the authors) would have increased. Conversely, Duguid and Scherer (2010) measured a carbonation gradient from the edge (rim) of the sample to the non-reacted zone while the brine was flushed around the core with a low value of the CO_2 partial pressure (0.1 MPa). Here, the results were similar to that observed in batch experiments (i.e. the formation of a calcite rim) because of both the low flushing rate and acidity of the fluid. The authors related the thickness of the altered rim, corresponding to a change in porosity, to exposure duration. Using batch experiments, Liteanu and Spiers (2010) showed that the permeability of fissured samples decreases due to fracture healing if the fractured cement sample subjected to supercritical CO_2 exposure, while Bachu and Bennion (2009) observed an increase of permeability when renewing the fluid around a fissured cement core. Yet, this result remain qualitative because the flow rate in the fissures was not controlled neither measured.

Hereafter we will investigate these mechanisms in the frame of a controlled continuous renewal of CO_2-rich fluid in a fracture. This situation is that expected when seepage is activated by the mechanical failure of the cement material that initially seals two layers of distinctly different pressure: the storage reservoir and the aquifer above the caprock, for instance. In this case, calcium carbonate layer formed from the portlandite and CSH dissolution (Eqs. (2) and (3)) can be re-dissolved by the carbonic acid contained in the flowing brine. This mechanism was described by Sauki and Irawan (2010) and Kutchko et al. (2007) from geochemical calculations and will be examined here using a set of flow-through experiments conducted on fractured cement sample reproducing in situ pressure and temperature conditions. Permeability changes are measured continuously during the experiment. The chemical and physical degradation of the cement as the function of the distance to the fracture are described *post mortem* using complementary analytical tools. Finally we compare these observations with the result of a simple diffusion – reaction transport model and study the displacement of the reaction fronts.

2. Materials and methods

2.1. Preparation and composition of cement samples

The cement material used in this work is a sulphate-high resistant Portland cement (SRPC), referenced CEMI 52.5 N CE CP2 NF, and was supplied by LAFARGE (Frangey production unit, France). The composition is given in Table 1. Cement slurry was obtained by mixing initial cement with fresh water using a standard water to cement ratio of 0.4.

The resulting slurry was then set using a syringe inside molds of 150 ml, and then closed during 4 months for curing and hydration. Long duration condition was chosen to reach advanced state of the hydrated paste. The slurry density is 1.85 g/l (15.41 mlb/gal), which is the density of cement slurry usually used for cementing well in the oil industry (Barron, 2009).

The composition of the cured cement is given in Table 1. XRD and thermogravimetry analysis results are similar to those obtained by numerical simulations using the speciation code GEMS (Kulik et al.,

Table 1
Chemical and phase composition for the Portland cement before (left) and after (right) hydration process (curing). TGA is for thermo-gravimetric analysis.

Normative phases (%)		Oxides (%)		Hydrated phases (%)	
Alite mono	56.7	SiO_2	19.04	CSH	46.0
Belite	18.5	Al_2O_3	5.85	Portlandite	23.0−TGA = 22.2
Ferrite	9.4	Fe_2O_3	2.45	Ettringite_Al	10.5
Cubic aluminate	7.9	CaO	63.11	SO_4_OH AFm	5.2
Ortho aluminate	1.8	MgO	1.69	OH-hydrotalcite	3.47
Lime CaO	0.5	K_2O	0.94	Hemicarbonate	8.9
$Ca(OH)_2$	0.8	Na_2O	0.05	Goethite	1.82
Periclase	0.4	SO_3	3.6	Calcite	1.02−TGA≅1.2
Quartz	0.1	TiO_2	0.31	Total	99.9
Calcite	1.2	Mn_2O_3	0.04		
Gypsum	0.4	P_2O_5	0.29		
Semi-hydrate	2.4	Cr_2O_3	<0.01		
Total	100.1	ZrO_2	0.04		
		SrO	0.11		
		LOI	1.91		
		Total	99.43		

2004) with the database CEMDATA07 (Lothenbach et al., 2008). Cylindrical samples (cores) of 9 mm diameter and 18 mm length were cored. One of the core was fractured along the main axis in order to obtain two halves of similar size. To obtain such a geometry mimicking a natural mechanically induced rough fracture, the core was installed into a device equipped of two coplanar blades. When approaching the value of the constraint required for the material to break, a mechanical shock was operated and the cylinder split into two halves. The two other cores were sawed along the main axis in order to create simple planar fracture. In both cases the aperture of the fracture was controlled by installing micrometric gauge sheets at the sample edges, and then the two halves were kept rigid by forming two wedges of resin reinforced by glass fibers along the sample length. We used Duralco 4525 epoxy resin for its stable mechanical properties up to 260 °C and its high resistance to aggressive inorganic chemicals. Accordingly, the fracture aperture was maintained constant at the longitudinal edges of the sample independently of the confining pressure and fracture dissolution as verified by Gouze et al. (2003) and Noiriel et al. (2007).

Three fractured samples (P1, P2 and P3) of distinctly different aperture using micrometric gauge sheet of 35 μm, 20 μm and 5 μm thickness for P1, P2 and P3 respectively were prepared following the previous approach. While P1 is a rough fracture (made by mechanical rupture), P2 and P3 are planar fractures (sawed). In Section 3.1 it will be shown that the corresponding effective hydraulic aperture were measured to be 27.0 μm and 13.6 μm for P1 and P2 respectively (i.e. 77% and 69% of the theoretical mechanical aperture respectively) while the hydraulic aperture for P3 could not be measured because being lower that the measurement threshold of 2.0 μm.

2.2. Cement structure

Cured cement microstructure have been investigated prior to CO_2 exposure to be compared with the state after CO_2 percolation. Fig. 1 shows that portlandite and CSH are the predominant hydrated phases as measured by XRD and thermal analysis. Anhydrous grains of alite (Ca_3SiO_5) and belite (Ca_2SiO_4), remained despite to the long curing duration (4 months). The major micro porosity ranges from 2 nm for the mineral matrix porosity to 2 μm for the capillary pores (Fig. 1). As reported by Houst (1992), accidental porosity could exist due to trapped air during cement-water mixing which was not expulsed by compaction. Here, the pore size of such accidental porosity ranges from tens to few hundreds of microns (Fig. 1B) and represent less than 5% of the total porosity. Also, we observed that the hydration process may be accompanied by the development of micro cracks (aperture less than 3 μm) around the dissolved grains. These fractures are isolated structures but we can assume their possible reactivation by acidic fluid flow diffusion.

2.3. Flow-through experiments

The apparatus constructed for performing flow of CO_2-rich brine through cylindrical cores (fractured or not) is shown in Fig. 2. A complete description of the system can be found in Luquot and Gouze (2009); here we briefly describe its functioning for matter of illustrating the experimental protocol.

The experimental device consists of: (1) a motorized dual-piston pump system that produces the flow of brine, (2) a motorized piston pump containing liquid-phase CO_2 cooled at 5 °C that deliver the amount of CO_2 required to reach the desired partial pressure,

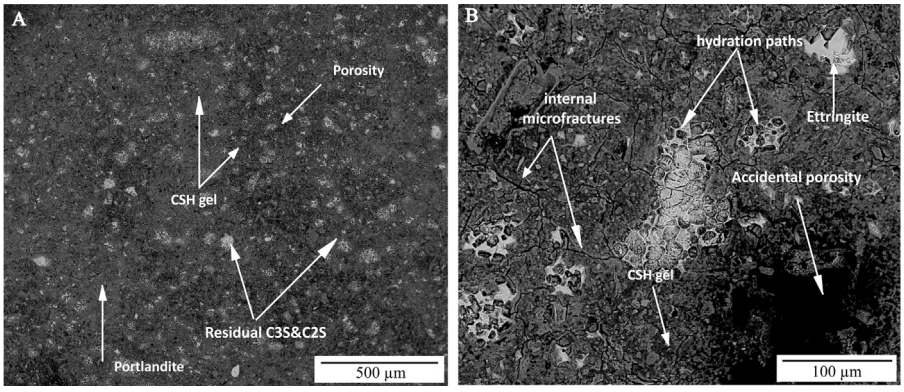

Fig. 1. Environmental scanning electron microscope images of a cement sample cured during 4 months. The images show that portlandite is embedded in microcrystalline (gel) CSH (A). Some minerals are not totally hydrated and large secondary pores are observed (B).

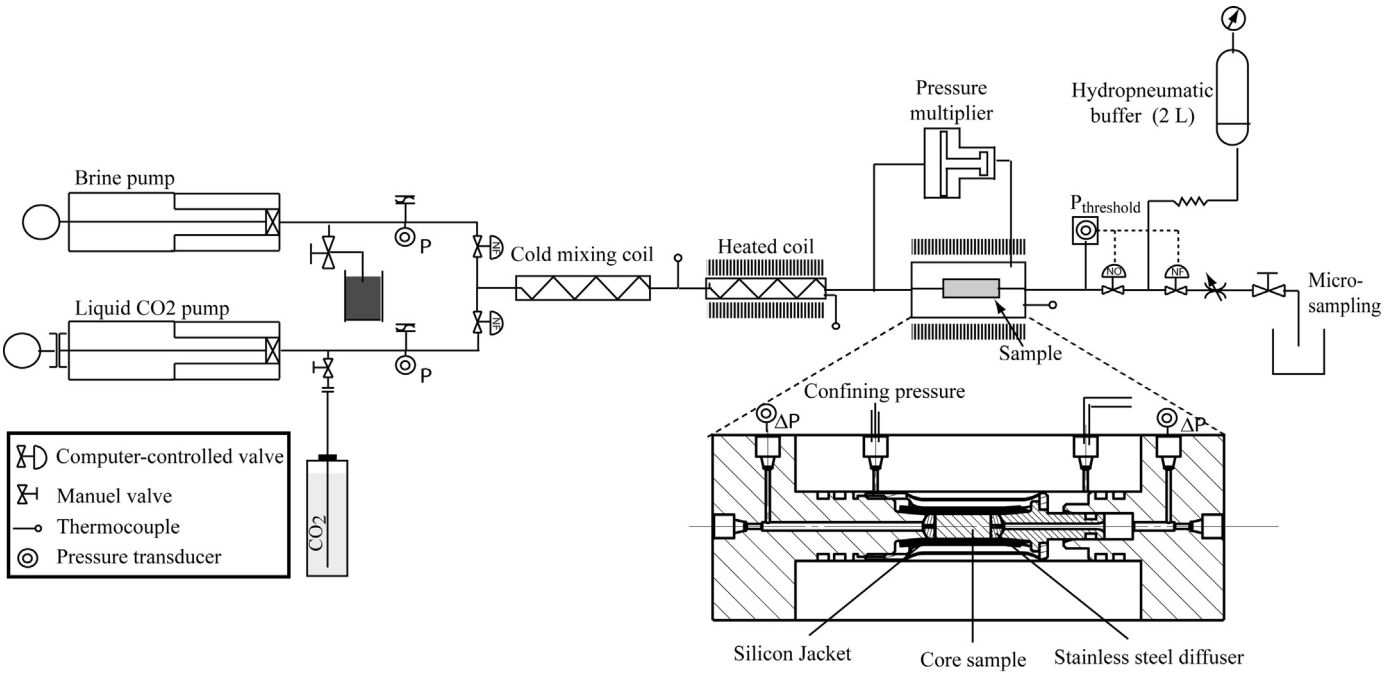

Fig. 2. Experimental setup with details of the core-holder confining cell. The temperature maintained at 5 °C details from the injection pumps to the cold mixing coil in order to have a liquid CO_2 phase. Conversely, the temperature is set to 60 °C from the heated coil mixing to the outlet sampling device.

(3) the CO_2-brine mixing system based on Taylor's dispersion in a 20 m long, 0.5 mm diameter tube, (4) the temperature-controlled confinement cell holding the sample, and (5) the system of servo-controlled valves and hydro-pneumatic tanks used to control the back-pressure and to deliver samples of the outlet fluid. The sample is installed in the confinement cell (Fig. 2) into a silicon jacket. A controlled confining pressure is applied to mimic natural confinement conditions and balance changes in the fluid injection pressure to avoid deviatoric stresses that may damage the sample irreversibly during pressure loading and unloading phases. In the experiments, axial and radial pressures were maintained at an equal value of 112% of the inlet pressure using a mechanical pressure multiplier.

Experiments were conducted at 60 ± 0.5 °C with a pore pressure of 10 ± 0.1 MPa. These conditions were considered as realistic for reproducing average conditions of fractured well cement casing at the reservoir depth for CO_2 storage operations. Initially the samples were saturated during 18 h (P = 10 MPa and T = 25 °C), injecting cement equilibrated brine, i.e. alkaline pH condition at flow rate Q = 0.2 mL/min. This cement-equilibrated brine was prepared by mixing 0.5 mol of NaCl and grounded cement in 1 L of deionized water. The fluid was mixed for 5 weeks and filtered before use. The analysis of this fluid showed that the main components were Ca and Si, with respective concentration of 235.60 mg L^{-1} and 0.39 mg L^{-1}.

Permeability tests were performed using this non-reactive brine at different flow rates. Then, the cement equilibrated brine was replaced by brine of composition mimicking limestone-equilibrated pore water. Swapping from the cement-equilibrated to the limestone reservoir-equilibrated fluid is operated by switching from one pump to the other without any pressure fluctuation. The calcite-equilibrated brine was obtained by dissolving 0.5 mol of NaCl and 0.053 mol of $CaCl_2$ in 1 L of deionized water equilibrated with atmospheric CO_2. The initial pH, of the equilibrated reservoir-brine was 7.22. Subsequently, CO_2 was added to the brine at constant flow rate to obtain a single phase fluid of CO_2 partial pressure equal to 4.7 MPa. As mentioned above, the CO_2-brine mixing results from dispersion in long, small diameter tube. The CO_2 rich-brine solution and the sample were rapidly heated to 60 °C. The solution pH dropped to 3.45 (calculated using the geochemical code PHREEQ-C (Parkhurst and Appelo, 1999). This configuration mimics a leakage through a fractured cement of the CO_2 saturated brine contained in a limestone reservoir used for CO_2 storage. After each experiment, the sample is removed quickly (less than 2 min) from the confining cell and is dried at room conditions.

For experiment P1 and P2 displaying the largest hydraulic apertures, the CO_2 saturated brine was injected into the sample at a constant flow rate of 2 ml min^{-1} (3.2×10^{-8} m^3 s^{-1}) for P1 and 0.2 ml min^{-1} (3.2×10^{-9} m^3 s^{-1}) for P2. Experiment duration was 5.5 h for P1 and 50 h for P2 and P3 experiments. Fluid samples were regularly collected at the outlet during experiment for performing chemical analysis.

For the P3 sample displaying a very low fracture aperture continuous flow rate was not possible and we applied intermittent flow conditions producing cycles of pressure build up (differential pressure up 1.645 MPa) to and draw down (differential pressure down to 0.785 MPa). In this condition, diffusion becomes the dominant transport mechanism and consequently this experiment is very similar to a batch experiment but with a very low water/rock ratio. Using the duration of the pressure draw down of each cycle we qualitatively evaluate the change in permeability of the fracture. The compilation of the three experiment conditions is given in Table 2.

2.4. Rock and fluid analysis

Fluid samples were regularly collected at the outlet. Each fluid sample was acidified with nitric acid. The concentration of major elements (Ca, Si, Fe, and Al) was measured using inductively coupled plasma atomic emission spectroscopy (ICP-AES).

A set of complementary analytical tools was used to perform a pertinent characterization of the samples before and after the experiments. Non-invasive 3D images were acquired at the European Synchrotron Research Facility (ESRF) using the X-ray Computed Micro-Tomography (XCMT) at the ID19 beam line. The protocols used here is identical to that described in details in Gouze et al. (2003) and Noiriel et al. (2007) for sample P1 and P3.

Table 2
Sample characteristics and flow conditions for the three experiments.

Test	Type	Initial fracture aperture (μm)	Roughness of fracture	Flow rate ($m^3\ s^{-1}$)	PCO_2(MPa)	Time (h)
1	P1	30.0	Rough	3.2×10^{-8}	4.7	5.5
2	P2	13.6	Plane	3.2×10^{-9}	4.7	50
3	P3	<2	Plane	1.6×10^{-9}	4.7	50

After the experiment, the samples were sawed, perpendicular to the fracture in two halves, using a blade diamond slow speed saw. Ethanol was used instead of water as lubricant to prevent dissolution and contamination of cement materials (Kutchko et al., 2007; Thiery et al., 2007). One halve was used for producing thin sections for analysis using an Environmental Scanning Electron Microscopy (ESEM). ESEM was performed under high vacuum mode with a FEI Quanta 200 instrument equipped with a field emission gun and a dispersive X-ray system. Raman spectrometry was used to characterize final mineral precipitation on thin sections. Raman spectrometry analyses were done using a LabRAM ARAMIS with a laser wavelength set at 473 nm.

The second halve of the sample was sawed into slices then crushed inside an agate mortar. The resulting powder was divided into two portions. One was used to measure the water content in the solid sample as well as CO_2 and calcium carbonates and hydrated cement phases ($Ca(OH)_2$ and CSH) by thermo-gravimetric analysis (TGA) and thermo-differential analysis (TDA) measuring the weight loss when increasing the temperature from room temperature to 1000 °C at a rate of 10 °C/min after validation with different temperature rates of 2 °C/min, 5 °C/min and 10 °C/min (Lothenbach et al., 2008).

The second portion of the powdered cement material was used for X Ray Diffraction analysis (XRD) to determine the mineral phases. Similar analyses (TGA–TDA and XRD) were performed on unaltered cement samples for direct comparison.

3. Results

The changes in the hydrodynamic properties of the fractured samples are related to dissolution and precipitation mechanisms. The following sections describe how chemical processes impact on hydrodynamic properties.

3.1. Permeability and fracture aperture.

Permeability measurements were performed by following the pressure drop (ΔP) between the inlet and outlet of the sample. The change in ΔP denotes the changes in the mean hydraulic aperture of the fracture caused by the ongoing hydro-chemical processes, because the cement material permeability is very low ($\leq 10^{-19}\ m^2$).

Here, we estimate the hydraulic aperture a_h and permeability k using the cubic law approximation (e.g. de Marsily, 1986):

$$a_h = \sqrt[3]{\frac{12\mu Q}{w\nabla P}} \tag{5}$$

and

$$k = \frac{a_h^2}{12} \tag{6}$$

where Q ($m^3\ s^{-1}$) is the flow rate, μ (Pa s) is the dynamic viscosity of the brine and w (m) the width of the fracture. In equation (5), the pressure gradient ∇P is the ratio of the pressures difference ΔP (Pa) between the fracture inlet and outlet and the fracture length L. Fig. 3 shows the time-resolve permeability for experiments P1 and P2. The permeability remains constant during experiment P1 (Fig. 3a) and increases slowly during experiment P2 (Fig. 3b). The final fracture permeability of sample P2 reaches $2.9 \times 10^{-11}\ m^2$.

As already mentioned, experiment P3 is close to a batch system (diffusion dominated transport) due to the low initial permeability of the fracture (fracture aperture < 2 μm). A continuous healing of the fracture (permeability decrease) is inferred from the observed decrease of the injection build up duration and associated increase of the draw down period with elapsed time (Fig. 4). These observations are similar to those reported by Liteanu and Spiers (2010) during batch experiments.

3.2. Fluid chemistry

Fig. 5 displays changes in the element concentrations during experiments P1 and P2. For both P1 and P2, the differential concentrations ΔC_{Ca} and ΔC_{Si} decrease, with $\Delta C_i = C_i|_{out} - C_i|_{in}$. The values of $\partial(\Delta C_{Ca},)/\partial t$ and $\partial(\Delta C_{Si})/\partial t$ decrease as well (Fig. 5). Lower differential concentration ΔC_{Al} and ΔC_{Fe} are obtained. We observe a concentration increase for both Fe and Al from $t = 0$ to $t \approx 100$ min for experiment P1 and to $t \approx 250$ min for experiment P2 and then a decrease until the end of the experiment. For all the duration of the experiment ΔC_{Ca}, ΔC_{Si}, ΔC_{Fe} and ΔC_{Al} were positive denoting that dissolution processes were dominant. Outlet concentrations of Ca and Si are higher during experiment P2 than P1, i.e. during low flow rate injection and with a planar sample fracture. Conversely,

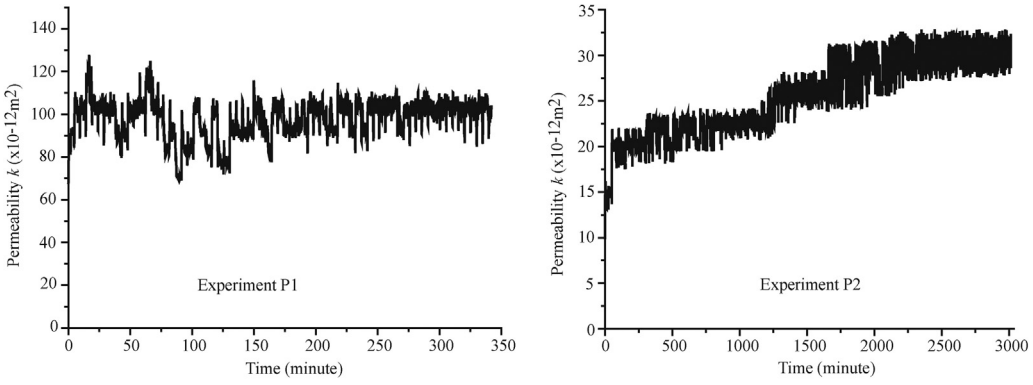

Fig. 3. Fracture permeability versus elapsed time measured during experiments P1 (left) and P2 (right).

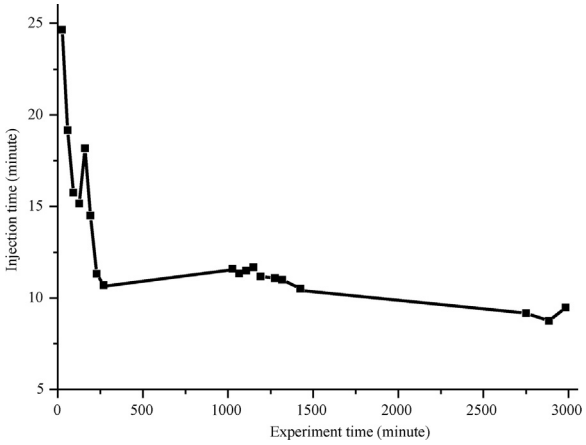

Fig. 4. Pulse duration required to increase pressure from 0.785 to 1.645 MPa as the function of the elapsed time. The decrease of the pulse duration denotes the decrease of the sample permeability.

the Fe and Al concentrations are lower during experiment P2 than P1.

3.3. Cement phase characterization

After experiment, non-reacted cement paste constitutes most of the sample for experiment P1, P2 and P3. Nevertheless, near the fracture distinct reactions can be observed (Fig. 6) for the three different samples. For sample P1, we noticed from the fracture to the non-reacted cement, (i) a high porosity zone of around 100 microns large (see Fig. 7); (ii) a dense zone with very low porosity of around 100 microns; (iii) a third zone with higher porosity than the second one but lower than the first one of around 50 microns and (iv) the non-reacted cement. Sample P2 and P3 display similar reactive zones except the first one with the high porosity, near the fracture. Comparable results were observed by Rimmelé et al. (2008), and Barlet-Gouédard et al. (2007) during cement cores exposed to CO_2-rich fluid under in situ conditions during batch experiments. The low porosity zone has the same size for experiments P2 and P3 and P1, but the third zone with high porosity is thicker than in sample P1 for both samples P2 and P3 (around 450 μm). The main mineral forming the low porosity zone can form locally round shape features such as nodules (Fig. 6) but generally the mineral phases fill the small fractures and form a uniform low porous grey zone. ESEM chemical analyses indicate that this mineral has the composition of a calcium-carbonate. Local ESEM analyses also indicate that the first zone with very high porosity observed in sample P1 is rich in amorphous materials composed of Si and Al (i.e. polymerized silica and Al-Si gels). The third zone with intermediate porosity is Ca depleted. This high porosity zone was identified in the previous studies where cement specimens were bathed with CO_2-rich fluid during batch experiments (Barlet-Gouédard et al., 2007; Rimmelé et al., 2008; Sauki and Irawan, 2010; Liteanu and Spiers, 2010) as well as during leaching experiments (Wigand et al., 2009; Bachu and Bennion, 2009; Duguid and Scherer, 2010).

The XRD analyses of the three samples indicate that calcite is the only Ca-rich secondary phase observed in the reacted samples. Raman spectrometry applied on thin sections also indicates that the low porous grey zone is mainly composed of calcite (Fig. 8). This result contrasts with the presence of aragonite and vaterite identified by Carey et al. (2007), Wigand et al. (2009), Rimmelé et al. (2008), and Corvisier et al. (2010). Conversely, it fit the observations did by Tai and Chen (1998) who indicated that vaterite does not precipitated at 60 °C, while aragonite precipitation occurs in presence of high Mg concentration (around 5 mM L^{-1}). In our experiments the inlet fluid is Mg free and the Mg content of the cement is very low (<1.7 wt.%). They also demonstrated that calcite is the main precipitated carbonate at high pH (here controlled by the cement pH). Also, it is worth noting that metastable carbonate species, such as

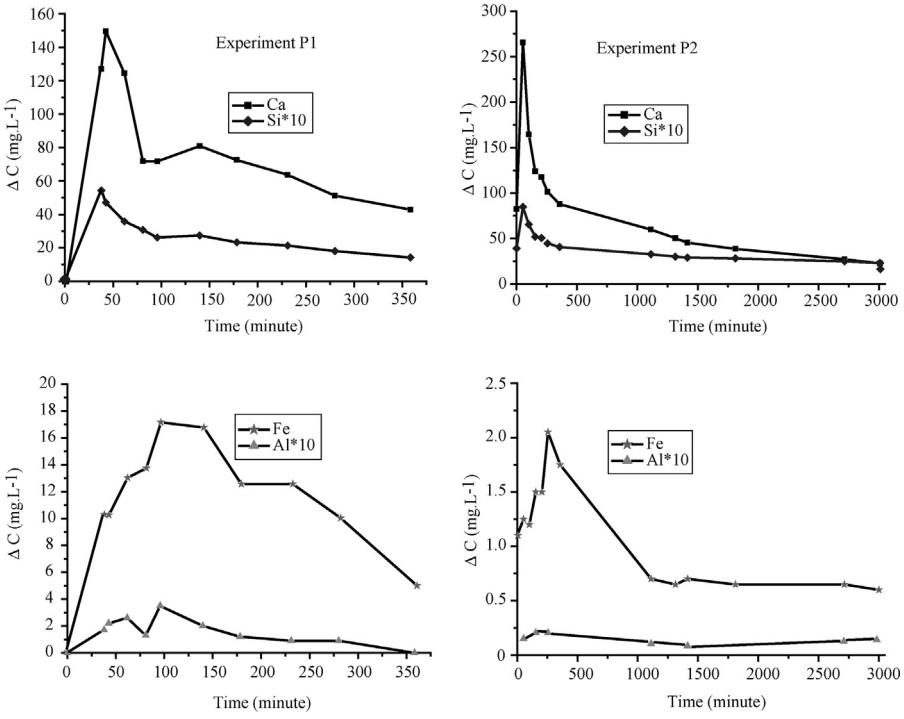

Fig. 5. Concentration versus time for experiments P1 (left) and P2 (right). Ca (square) and Si (diamond) concentrations are showed on the top whereas, Fe (star) and Al (triangle) in the bottom. Si and Al concentration are multiplied by ten for better visualization.

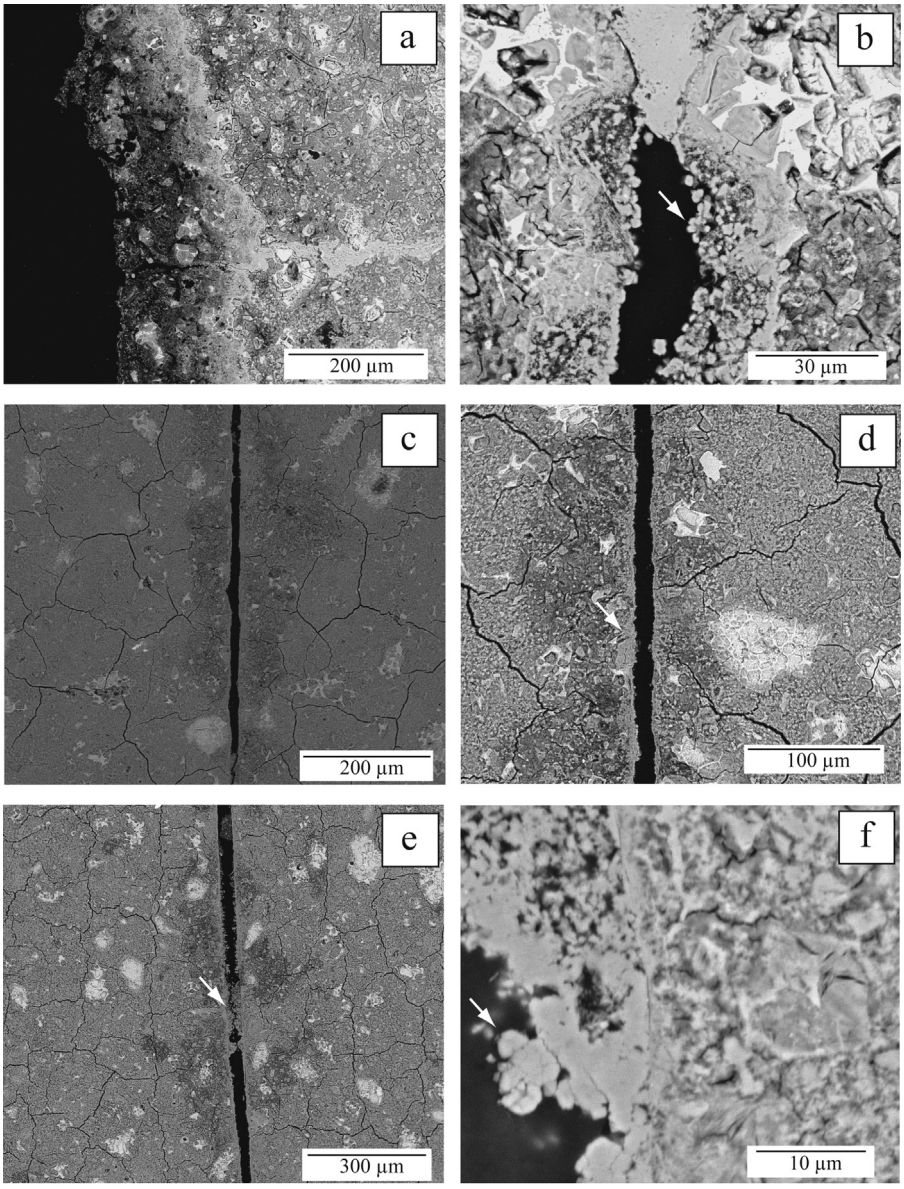

Fig. 6. Environmental scanning electron microscope images of samples P1 (top), P2 (middle) and P3 (bottom) after CO_2-rich brine injection experiments. Figure a (sample P1), c (sample P2) and e (sample P3) display the fracture and the different reaction zones. Figure b (sample P1, in secondary fracture) and f (sample P3) show the formation of calcite nodules where diffusion is dominant. The calcite precipitation into the main fracture is clearly visible in figure d (sample P2) and e (sample P3). The local clogging of the main fracture by calcite precipitation is marked by an arrow in figure e.

vaterite and aragonite, should be first re-dissolved by the CO_2-rich brine flowing in the fracture.

Results presented in Fig. 9 show the mass loss of phases as function of heating temperature before and after CO_2 rich brine percolation using TGA–TDA techniques. Mass loss occurs in three stages. The first stage characterized before and after experiment within the temperature ranges (0–110 °C and 110–350 °C) characterizes the evaporation of free water and dehydration of CSH and ettringite. The mass lost in this domain is highlighted by the first peak of the TDA curve. The second stage taking place from 350 to 470 °C is related to the dehydration of portlandite [$Ca(OH)_2$) = $CaO + H_2O$]. As displayed in the Fig. 6, the quantification of the mass loss in this temperature range is quite easy to handle as portlandite appears to be the unique phase implicated. Finally, the decarbonation of calcite due to CO_2 mass loss occurs at 530 °C as reported by Villain et al. (2007).

4. Discussion

4.1. Mass balance

Because of the very low fluid injection during experiment P3, we could not sample fluids for chemical analyses. Consequently we will discuss the chemistry results for experiments P1 and P2 only.

As presented in Section 3.2 the differential concentrations ΔC_i are positive for all the cations (Fig. 5). The release of Ca results from the dissolution of CSH, portlandite and ettringite. The lower release of Fe is attributed to the dissolution of goethite and the release of Al from ettringite while the release of Si results from the dissolution of CSH (see Table 1).

For both experiments P1 and P2, the outlet water is depleted in Si yet enriched in Ca compared to the composition expected from the stoichiometric dissolution of CSH and CH (Fig. 10). Two hypotheses

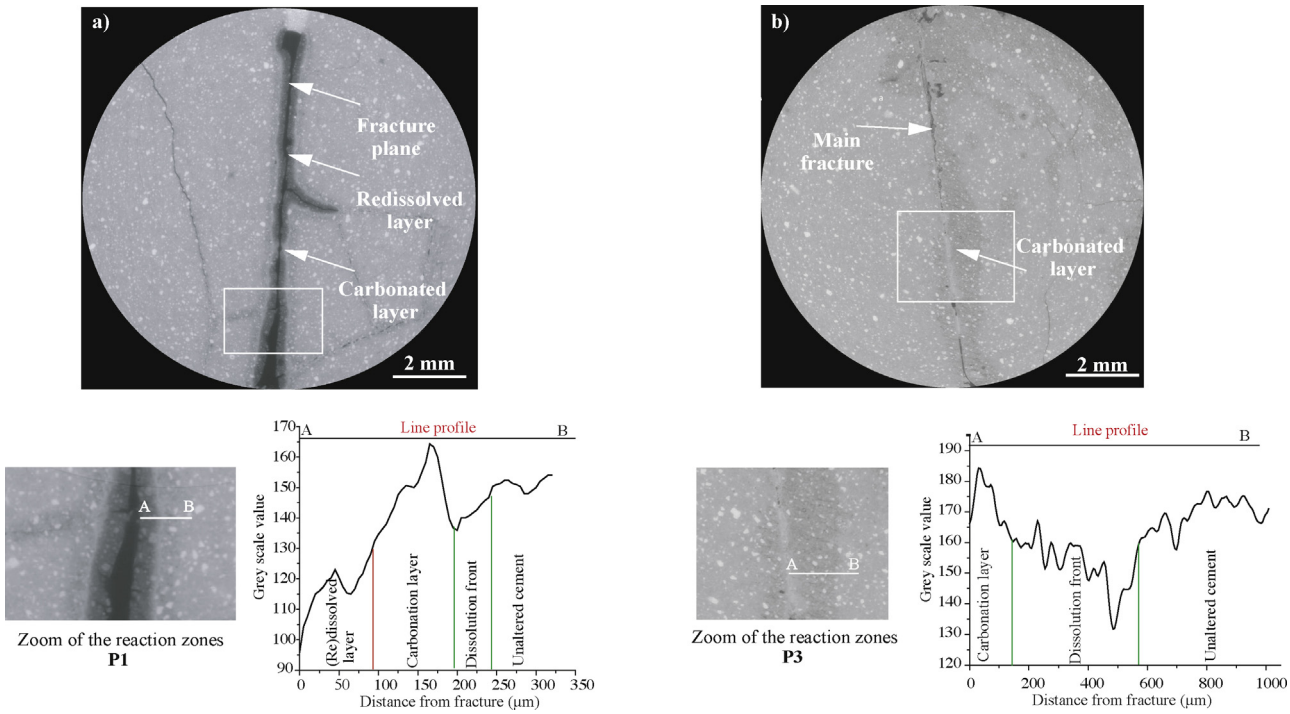

Fig. 7. Top: Numerical cross section of X-ray microtomography images performed after experiments for P1 (left) and P3 (right). Bottom: X-ray attenuation (grey levels) profile perpendicular to the fracture.

can explain the high Ca/Si ratio in the outlet fluid, (i) Si-rich mineral precipitates inside the sample, (ii) the portlandite mineral is more dissolved than CSH. We can also notice in Fig. 10 than during experiment P1 the Ca/Si ratio remains constant during all the experiment (around 20) whereas for experiment P2 the Ca/Si ratio decreases from 20 to 7.5 at the end of the experiment. At the beginning the Ca/Si ratio is the same in both experiments but the effective Ca and Si concentrations are twice for experiment P2 compared to P1. This indicates that CSH is more dissolved in experiment P2 (lower flow rate and plane fracture) than in P1, at least at the beginning of the experiment. TGA–TDA analyses confirm that a higher quantity of portlandite was dissolved during experiment P1 (decrease from 4.4% to 3.9% for experiment P1, to 4.1% for experiment P2 and to 4.2% for experiment P3, Fig. 9).

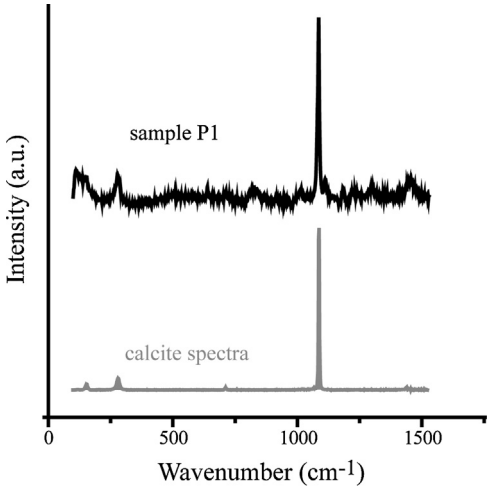

Fig. 8. Raman spectroscopy analysis showing that calcite is the only polymorph of $CaCO_3$ precipitated. This spectrum was acquired on sample P1 after experiment.

Nevertheless, this difference in portlandite dissolution cannot explain the high difference in Ca/Si ratio. The only assumption to explain the difference in the Si depletion between P1 and P2 is the precipitation of Si-rich mineral. Fig. 6 shows clearly that during experiment P1 a very porous zone appears in contact with the fracture whereas it is not observed for experiments P2 and P3. This zone has a high porosity and it is almost completely composed of Si, Na and Al. During X-ray microtomography acquisition we noticed a dehydration process due to the high beam energy which induces the formation of micro-crack in this highly porous zone as observed in Fig. 7. We conclude that this zone should have been more hydrated before the sample was extracted from the confinement and X-rayed. TGA–TDA analyses corroborate this hypothesis. Fig. 9 shows that the quantity of CSH and other hydrates decreases after CO_2 percolation for P2 whereas the quantity of hydrates increases for P1. This confirms that a hydrated Si-rich phase, probably an amorphous silicate phase, precipitates during experiment P1 near the fracture.

During the three experiments, even if the Ca concentration is higher in the outlet fluid than expected by stoichiometric dissolution, we identified the precipitation of calcite.

The amount of CO_2 released, measured by TGA–TDA, is 2.9 wt.%, 3.0 wt.% and 2.7 wt.% respectively for experiments P1, P2 and P3. Subtracting the initial calcite quantity (1.97 wt.%) we can calculate the quantity of precipitated calcite in each sample using the equation:

$$\%w_{CaCO_3} = \frac{(n_{CO_2} * M_{CaCO_3}) * 100}{m_{samp}} \quad (7)$$

where n_{CO_2} is the mole number of carbon dioxide measured by TGA, M_{CaCO_3} is the molar mass of calcium carbonates and m_{samp} is the sample mass (2 ± 0.05 g for each of the samples). We calculated that the $CaCO_3$ precipitated in each sample is 4.62 wt.%, 4.84 wt.% and 4.16 wt.% respectively for P1, P2 and P3.

Assuming that carbonation reaction is constant all over the experiment, we calculated a carbonation

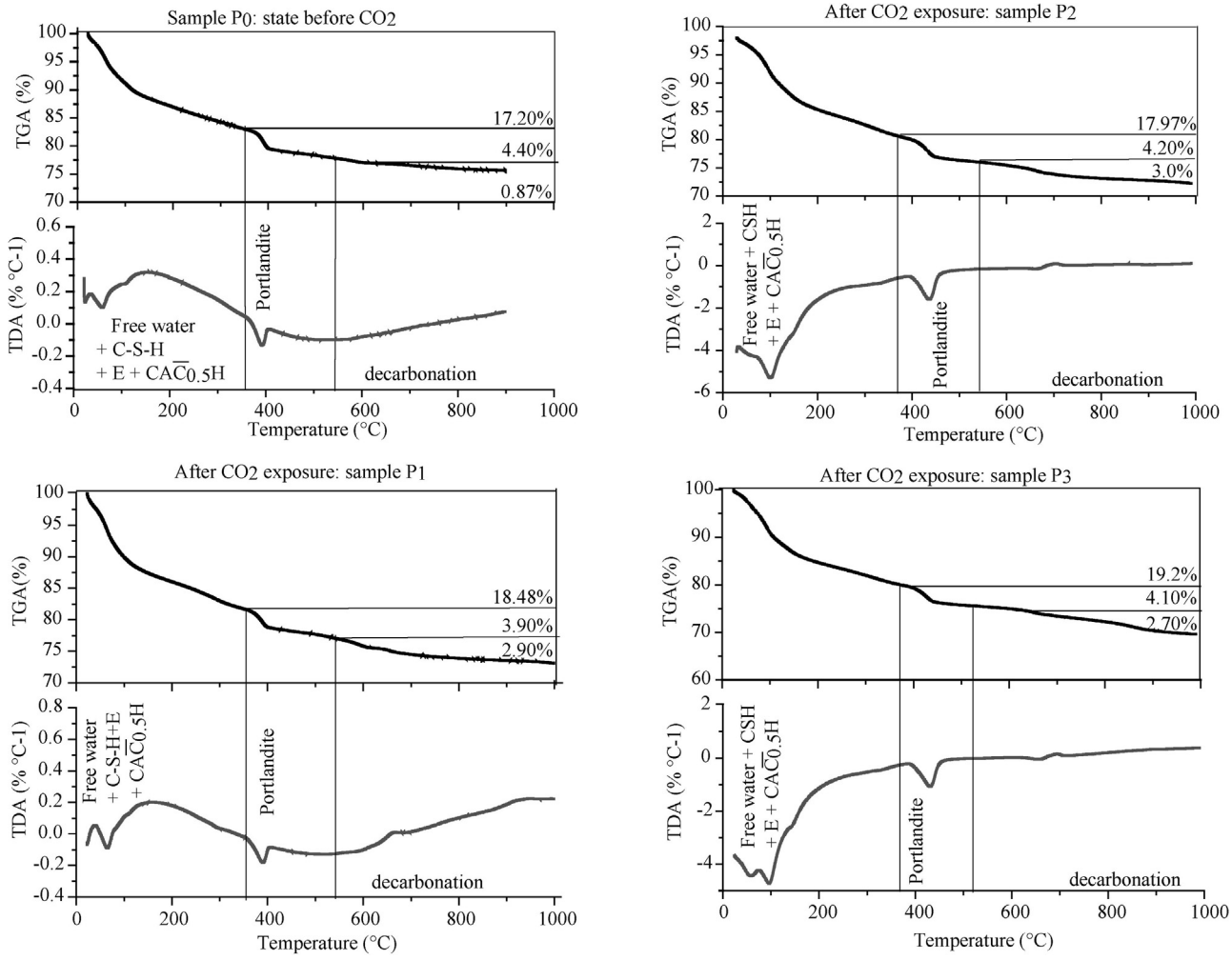

Fig. 9. TGA–TDA analysis before experiment (sample P0) and after experiment P1, P2 and P3. For each sample, the top graph displays the weight loss percent during the heating process and the bottom graph shows the temperature difference. These two variables allow identifying the different mineral phases.

rate of 7.0×10^{-3} wt.% mL^{-1}, 8.1×10^{-3} wt.% mL^{-1} and 320×10^{-3} wt.% mL^{-1} and concluded that the slower the flow rate is, the more efficient the carbonation process is.

4.2. Control of the flow rate on mass transfers and fracture permeability

In both flow-through experiments P1 and P2, we observed a decrease of the outlet cations concentration. This decrease denotes the lessening of the reaction products flux at the fracture surfaces controlled by the increase of both the distance between the reaction front and the fracture, and the thickness of the carbonation layer. Yet, while the concentrations seem to converge to similar value at large time, experiment P2 displays higher concentration than P1 for which the flow rate was ten times higher. Moreover we measured a higher quantity of precipitated calcite in experiment P2 than in experiment P1. For the lower flow rate (P2) only two reaction zones (the portlandite/CSH dissolution zone with low Ca

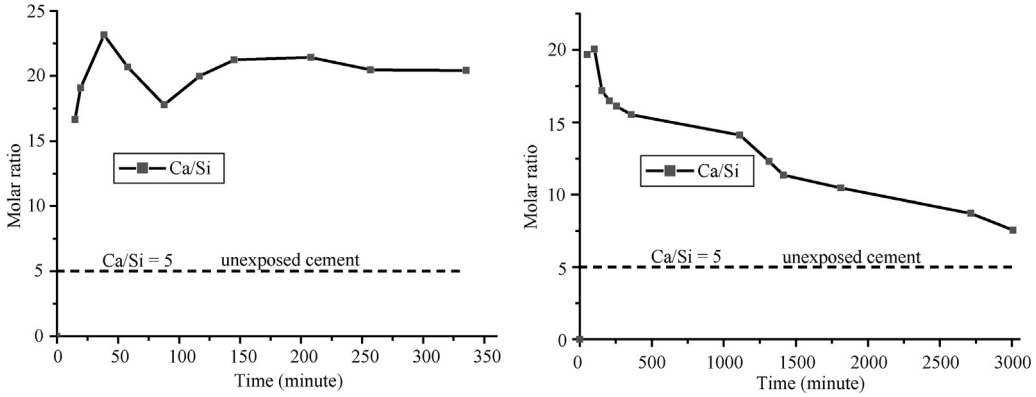

Fig. 10. Ca/Si ratio in the outlet fluid for experiment P1 (left) and P2 (right) versus elapsed time. The horizontal lines at Ca/Si = 5 represent the Ca/Si ratio in the initial cement sample.

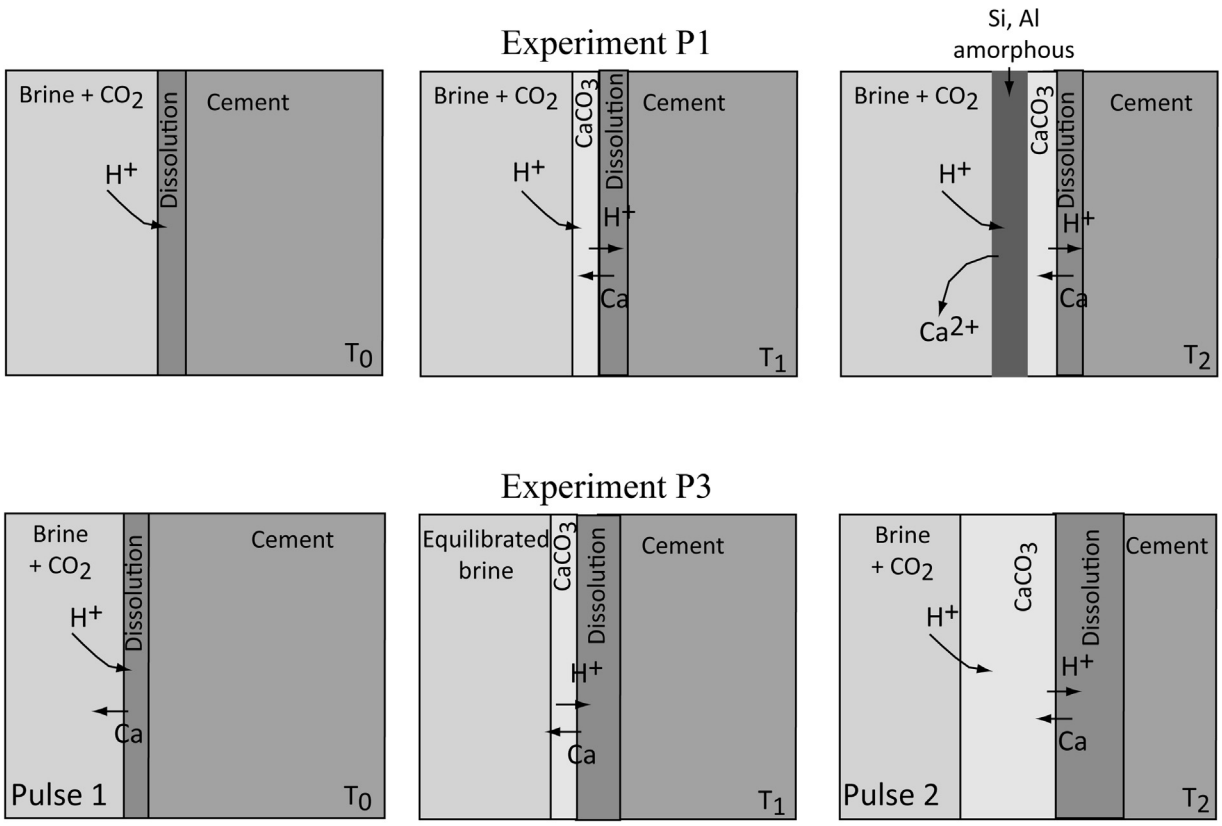

Fig. 11. Schematic description of the reaction processes which occurred during experiment P1 (top part) and P3 (bottom part).

and high porosity and the neoformed calcite layer) were described whereas we characterized a third zone with a very high porosity almost composed of Si–Al amorphous phases for the highest flow rate experiment (P1). This suggests that during experiment P1 the carbonation induced by the CH and CSH dissolution is accompanied by calcite re-dissolution because of the high renewal of the acidic fluid in the fracture. The calcite precipitation front progresses into the sample while the Si–(Al) amorphous phase grows within the re-dissolution zone (Fig. 6). Similar phenomena were described by Kutchko et al. (2009) and Duguid and Scherer (2010) at the surface of cylindrical samples strongly flushed by acidic flow. At the opposite we conjecture that during experiments P2 and all the more experiment P3 that both display only two reactions zones and thicker calcite layer than for P1. We can suggest that the renewal of the acidic fluid by diffusion was too weak to promote noticeable calcite re-dissolution (Fig. 11). Such increase of the calcite precipitation zone was observed by Carey et al. (2007), Bachu and Bennion (2009) and Liteanu and Spiers (2010). Moreover, we observed that during experiment P1 (high flow rate) carbonation process and healing occurs in pre-existing cracks perpendicular to the main fracture, i.e. dead end structures where fluid renewing is controlled by diffusion (Figs. 6, 7 and 11). This confirms that the re-dissolution of the calcite and the formation of Si-rich layer can only take place if the flux of acidic fluid is high and induce a penetrating acidification of the cement matrix.

During experiment P1, the permeability remains constant despite the redissolution of the neoformed calcite layer (Fig. 3), whereas Bachu and Bennion (2009) observed an increase of the apparent fracture aperture (permeability was not measured by the authors) for experiments with initially large apertures (10 μm–300 μm). Here we claim that the formation of the micro-porous Si-rich layer in the vicinity of the fracture allows maintaining the initial fracture aperture and consequently the permeability. Conversely, the permeability decrease due to the calcite precipitation for experiment P3 (similar to batch conditions) as it was observed by Rimmelé et al. (2008), Barlet-Gouédard et al. (2007), Bachu and Bennion (2009), Wigand et al. (2009), Carey et al. (2007), and Liteanu and Spiers (2010). We can see in Figs. 6 and 7, that the precipitation of calcite almost totally healed the fracture.

During experiment P2 with intermediate flow rate, permeability increases slowly from 20 to 30 D from $t = 0$ to $t = 2000$ min and then remains almost constant to the end of the experiment (Fig. 3) similarly to what was reported by Wigand et al. (2009). The increase of permeability, i.e. an increase of the hydraulic aperture, can be related to the low porosity (high density) of the carbonation compared to that of the hydrated minerals but also to the noticeable withdrawal of mass observed during the first half of the experiment duration. The constant permeability at the end of the experiment associated with the low and stable cation withdrawal (Fig. 5) denotes the attainment of a metastable regime where the volume transfers between dissolved and precipitated minerals compensate.

4.3. Numerical modeling

We modeled the diffusion of the reactants and products from the fracture to the cement bulk (Huet et al., 2010). Corvisier et al. (2010) and Geloni et al. (2011) stated that portlandite is the main mineral dissolved during CO_2 exposure (the dissolution of minor quantity of CSH were also reported). Accordingly, and because the thermodynamic and kinetic constants for CSH are unknown, we will assume that only portlandite is the reactive phase in the initial cement.

The simulations were carried out using the reactive geochemical code PHREEQ-C (Parkhurst and Appelo, 1999). In the cement, fluid transport is driven by diffusion. The SIT database was modified to take into accounts only species and phases related to portlandite and calcite dissociation–precipitation. Solid phases were

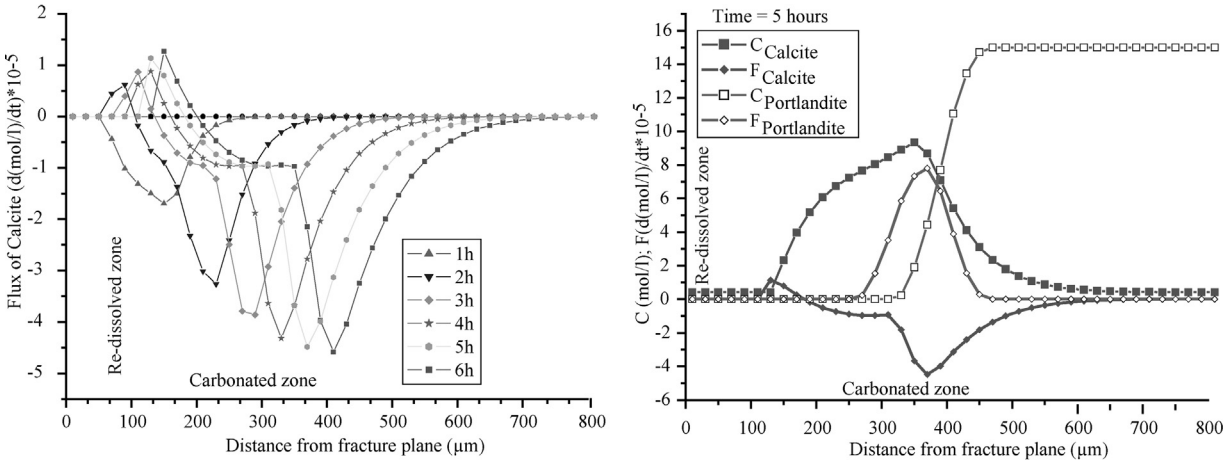

Fig. 12. Numerical modeling corresponding to experiment P1. Left: Calcite dissolution ($F>0$) and precipitation ($F<0$) rate versus the distance to the facture for different elapsed time t. Right: Calcite and portlandite concentration and mass exchange rate versus the distance to the fracture at $t=5$ h (i.e. corresponding to the duration of experiment P1).

allowed to dissolve and precipitate according to a kinetic rate based on transition state theory defined by Lasaga and Kirkpatrick (1981). Kinetic constant for portlandite dissolution was set to 6.4×10^{-6} mol/m^2 s^{-1}, as reported by Halim et al. (2005) and Geloni et al. (2011) and measured by Regnault et al. (2009). The kinetic model for calcite dissolution and precipitation was modified from Plummer et al. (1978), to enable carbonates re-dissolution. We used the calcite kinetic constant of precipitation (3.5×10^{-7} mol/m^2 s^{-1} measured at $T=54.5\,^{\circ}$C), calculated by Brecevic and Kralj (2007) and applied by Corvisier et al. (2010). The geochemical reaction equations are solved by a Newton–Raphson iterative method.

Diffusion coefficient was set to 0.7×10^{-12} m^2 s^{-1}. This is an intermediate value between that simulated by Bentz et al. (2000) (1.3×10^{-12} m^2 s^{-1}) and the one calculated from the Japan Society of Civil Engineers definition related to cement with $W/C=0.4$, obtained to 3.38×10^{-14} m^2 s^{-1}. For initial condition, we set the initial cement porosity at 19%, (evaluated from the mercury intrusion measurements), the calcium concentration in the cement pore water at 28 mmol/L (water equilibrated with portlandite) and the pH at 12.57 (calculated as equilibrated pH at $T=60\,^{\circ}$C). We discretize (one-dimension mesh) the cement from the fracture ($x=0$) to twice the distance corresponding to the observed mass transfers using 105 cells of 10 microns resolution and added increasingly larger cells in order to simulate a semi-infinity system and make the mass transfers in the vicinity of the fracture independent from the $x>0$ boundary condition (Huet et al., 2010).

This one-dimension diffusion-reaction model was applied here to experiments P1 and P3, i.e. for the high flow rate injection of CO_2-rich brine and for the diffusion control experiment. Results for P1 are displayed in Fig. 12, where C_i and F_i denote the concentration and the dissolution rate ($F_i>0$ corresponds to dissolution) for mineral i respectively. The model reproduces fairly the position of the three different reaction zones controlled by Eqs. (2) and (4): portlandite dissolution ($F_{\text{portlandite}}>0$), calcite precipitation ($F_{\text{calcite}}<0$) and calcite redissolution ($F_{\text{calcite}}>0$). The carbonated zone corresponds then to the remaining calcite controlled by precipitation and dissolution. As time increases, this front progresses inside the cement. Its thickness increases because the precipitation rate appears to be higher than the dissolution flux (Fig. 12).

For experiment P3, where carbonation process tends to heal the fracture, the model reproduces the two main reaction zones, i.e. the portlandite dissolution and the calcite precipitation. As expected calcite redissolution is not observed, but more importantly the model predicts a rate of calcite precipitation about three times higher than for experiment P1. Consequently, the quantity of precipitated calcite is higher for batch experiment conditions (experiment P3, Fig. 13) than during high flow rate renewal in the fracture (experiment P1, Fig. 12), as observed during the experiments.

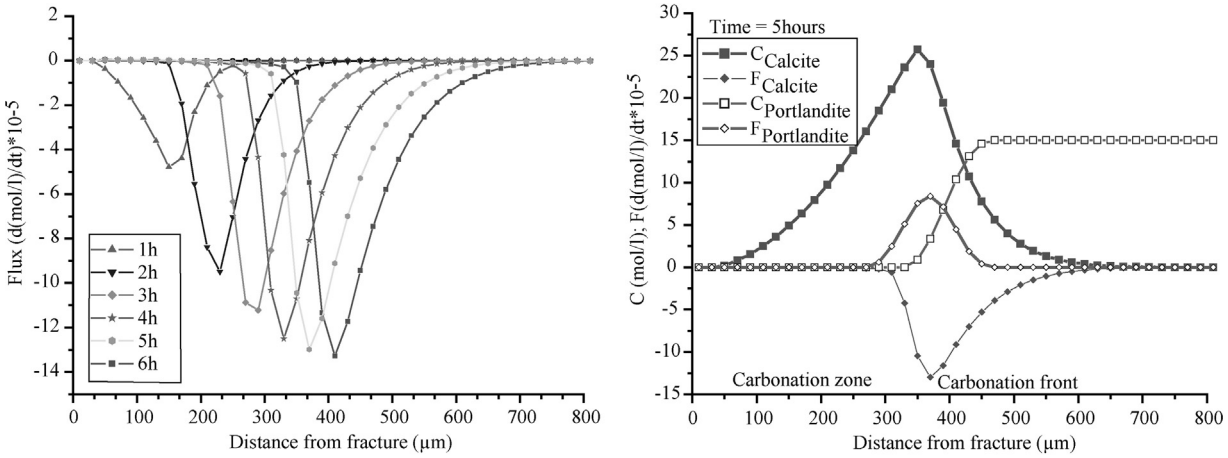

Fig. 13. Numerical modeling corresponding to experiment P3. Left: Calcite precipitation ($F<0$) rate versus the distance to the fracture for different elapsed time t. Right: Calcite and portlandite concentration and mass exchange rate versus the distance to the fracture at $t=5$ h.

Yet, it is worth noticing that for both models the thickness of the reaction zones is measurably higher than the observations, while the time resolved position is well modeled. This inaccuracy of the model – that cannot be mitigated by tuning the parameters, for instance the kinetic coefficients – leads to the assumption that the reactive hydrated mineral is portlandite only whereas it represents less than one quarter of the cement mass (see Table 1). Though, portlandite carbonation is known to be more efficient than CSH carbonation (Calleja (1980) and Houst (1992)), albeit the thermokinetic constants for CSH and they control on the fluid speciation are poorly known.

4.4. Consequences of CO_2-rich brine leakage

These experimental results indicate that the fracture permeability changes of a Portland cement flowed by CO_2-rich brine depend mainly on the initial fracture aperture. If the fractured aperture is small (experiment P3), leakage would be mitigated by calcite precipitation that rapidly fill the fracture. Similar mechanism is expected in secondary cracks and dead-end fractures connected to the main flowing fractures (experiment P1).

Conversely, larger fractures promote an efficient renewing of the acidic brine at the fracture walls that triggers calcite re-dissolution and the formation of a Si-rich amorphous layer in contact with the fracture void. However the net mass balance indicated matter removal during all the experiment duration while permeability measurements indicate that in this case leakage may sustain (experiment P1).

5. Conclusions and perspectives

So far, cement alteration was principally studied experimentally using batch reactor (with static or renewed fluid), CO_2-enriched brine (usually with pH lower than 5) and reservoir conditions. All these experiments exhibit similar carbonation mechanisms and authors associate them with an ubiquitous reduction of porosity and permeability (Rimmelé et al., 2008; Wigand et al., 2009; Bachu and Bennion, 2009; Liteanu and Spiers, 2010).

However, mechanical failure of the cement material that initially seals two layers of distinctly different pressure may occurs due to mechanical stresses. In this case the fluid saturated the porous reservoir may leak through the fracture. Depending on the distance to the injection well and residence time of the fluid in the vicinity of the fracture inlet, either CO_2-rich brine or supercritical CO_2, or both, can be withdrawn by the fracture. Here we investigated the cement alteration mechanisms in the frame of a controlled continuous renewal of CO_2-rich fluid in a fracture, which is view as the most reactive situation.

We investigated the effect of flow rates from quasi-static flow (experiment P3) to higher flow rates for well-connected fractures (experiment P1 and P2). In the quasi-static case we observed an extensive conversion of portlandite ($Ca(OH)_2$) and calcium-silicate-hydrate (CSH) to calcite ($CaCO_3$) in the vicinity of the fracture similar to that observed in the published batch experiments. Eventually, the fracture was almost totally healed.

The experiments with constant flow revealed different behavior triggered by the continuous renewing of the reactants and withdrawal of reaction products. We showed that calcite precipitation is more efficient for low flow rate. With intermediate flow rate (experiment P2), we measured that permeability increases slowly at the beginning of the experiment and then remains constant due to calcite precipitation in replacement of CSH and CH into fracture border. With higher flow rate (experiment P1), we measured a constant permeability which can be explained by the development of a highly hydrated Si-rich zone which maintains the initial fracture aperture during all over the experiment while noticeable mass is released from the sample.

Numerical simulations performed for experiments P1 and P3 reproduce the different reaction zones observed during experiments using standard thermodynamic and kinetic database. A re-dissolved calcium carbonates layer appears clearly followed by non-dissolved calcite for experiment P1. However, the model overestimates the calcite precipitation most probably because the CSH dissolution is not negligible as we have had to assume (because of the lack of thermodynamic and kinetic data for these *P* and *T* conditions). Indeed, CSH are representing the major calcium source and would control the long term mass transfer dynamics, even though portlandite will control the system while present in the material. Consequently, the total precipitated calcite evaluated by numerical modeling is over estimated.

These preliminary results emphasize that more complex behaviors than those expected from batch experiments may take place in the vicinity of flowing fractures. We demonstrated that if only micro-cracks appear in the cement well, carbonation reaction may heal these micro-cracks and mitigate leakage whereas conductive fractures allowing high flow may represent a risk of perennial leakage. But, the experiments indicate that the precipitation of Si-rich amorphous phases may maintain the initial fracture aperture and limit the leakage rate. The long term efficiency of this amorphous low density material to maintain the fracture aperture must now be proved by performing long-lasting experiments at different follow rate in order to test its resistance to hydrodynamic erosion and changes in the alteration rate. Also, similar experiments than those presented in this paper must be performed using the standard corrosion resistant, low viscosity portland cements (known as class G cement) used in oil and gas industry.

Acknowledgements

This work was supported by the MUSTANG project (European Community FP7/2007–2013 under grant agreement no. 227286) and by the French Research National Agency (ANR) through the *Captage et stockage du CO_2* program (project CO-LINER no. ANR-08-PCO2-004).

References

Andreani, M., Gouze, P., Luquot, L., Jouanna, P., 2008. Changes in seal capacity of fractured claystone caprocks induced by dissolved and gaseous CO_2 seepage. Geophysical Research Letters 35, L14404, http://dx.doi.org/10.1029/2008GL034467.

Bachu, S., Adam, J.J., 2003. Sequestration of CO_2 in geological media in response to climate change: capacity of deep saline aquifers to sequester CO_2 in solution. Energy Conversion and Management 44, 3151–3175.

Bachu, S., Watson, T.L., 2006. Possible indicators for potential CO_2 leakage along wells. In: Gale, J.J., Rokke, N., Zweigel, P., Svenson, H. (Eds.), Proceedings of the 8th International Conference on Greenhouse Gas Control Technologies. Elsevier, Trondheim, Norway (CD ROM).

Bachu, S., Celia, M.A., 2009. Assessing the potential for CO_2 leakage, particularly through wells, from geological storage sites. In: McPherson, B.J.O.L., Sundquist, E. (Eds.), The Science of CO_2 Storage. Geophysical Monograph Series GM183. American Geophysical Union, Washington, DC.

Bachu, S., Bennion, D.B., 2009. Experimental assessment of brine and or/CO_2 leakage through well cement at reservoir conditions. International Journal of Greenhouse Gas Control 3, 494–501.

Barlet-Gouédard, V., Rimmelé, G., Porcherie, O., Quisel, N., Desroches, J., 2009. A solution against well cement degradation under geological storage environment. International Journal of Greenhouse Gas Control 3, 206–216.

Barlet-Gouédard, V., Rimmelé, G., Goffé, B., Porcherie, O., 2007. Well technologies for co$_2$ geological storage: CO_2-resistant cement. Oil and Gas Science and Technology 62, 325–334.

Barlet-Gouédard, V., Rimmelé, G., Goffé, G., Porcherie, O., 2006. Mitigation Strategies for the Risk of CO_2 Migration through Wellbores. Society of Petroleum Engineers, Miami, USA (IADC/SPE 98924).

Barron, A.R., http://creativecommons.org/licenses/by/2.0/Connexions module: m16444.Version 1.10 (26.06.09) 7:42 pm GMT-5

Bentz, D.P., Jensen, O.M., Coats, A.M., Glasser, F.P., 2000. Influence of silica fume on diffusivity in cement-based materials. Cement and Concrete Research 30, 953–962.

Bouc, O., Audigane, P., Bellenfant, G., Fabriol, H., Gastine, M., Rohmer, J., 2009. Determining safety criteria for CO_2 geological storage. Energy and Procedia 1, 2439–2446.

Brecevic, L., Kralj, D., 2007. On calcium carbonates: from fundamental research to application. Croatica Chemica Acta 80, 467–484.

Calleja, J., 1980. Durability. In: Proc. 7th International Congress of Chemical Cement, vol. I, Paris 1980, Ed. Deptima, pp. VII-2/1–2/48.

Carey, J.W., Wigand, M., Chipera, S.J., WoldeGabriel, G., Pawar, R., Lichtner, P.C., Wehner, S.C., Raines, M.A., Gurthrie Jr., G., 2007. Analysis and performance of oil well cement with 30 years of CO_2 exposure from SACROC Unit, West Texas, USA. International Journal of Greenhouse Gas Control 1, 75–88.

Celia, M.A., Bachu, S., Norbotten, J.M., Gasda, S.E., Dahle, H.K., 2004. Quantitative estimation of CO_2 leakage from geological storage: analytical models, numerical models and data needs. In: Proceedings of the 7th International Conference on Greenhouse Gas Control Technologies (GHGT-7), http://uregina.ca/ghgt7/PDF/papers/peer/228.pdf

Corvisier, J., Brunet, F., Fabbri, A., Bernard, S., Findling, N., Rimmelé, G., Balet-Gouedard, V., Beyssac, O., Goffe, B., 2010. Raman mapping and numerical simulation of calcium carbonates distribution in experimentally carbonated Portland-cement cores. European Journal of Mineralogy 22, 63–74.

Crow, W., Williams, D.B., Carey, J.W., Celia, M., Gasda, S., 2009. Wellbore integrity analysis of a natural CO_2 producer. Energy and Procedia 1, 3561–3569.

de Marsily, G., 1986. Quantitative Hydrogeology. Academic Press, San Diego, CA, USA440.

Deremble, L., Loizzo, M., Huet, B., Lecampion, L., Quesada, D., 2011. Stability of a leakage pathway in a cemented annulus. Energy and Procedia 4, 5283–5290.

Duguid, A., Radonjic, M., Scherer, G.W., 2006. The Effect of Carbonated Brine on the Interface between Well Cement and Geologic Formations under Diffusion-Controlled Conditions. 8th International Conference on Greenhouse Gas Control Technologies, Trondheim, Norway.

Duguid, A., Scherer, G.W., 2010. Degradation of oil well cement due to exposure to carbonated brine. International Journal of Greenhouse Gas Control 4, 546–560.

Ellis, B., Peters, C., Fitts, J., Bromhal, G., McIntyre, D., Warzinski, R., Rosenbaum, E., 2011. Deterioration of a fractured carbonate caprock exposed to CO_2-acidified brine flow. GHG Sciences and Technologies 1, 248–260.

Geloni, C., Giorgis, T., Batistelli, A., 2011. Modeling of rock and cement alteration due to CO_2 alteration in an exploited gas reservoir. Transport in Porous Media, http://dx.doi.org/10.1007/s11242-011-97140.

Gouze, P., Noiriel, C., Bruderer, C., Loggia, D., Leprovost, R., 2003. X-ray tomography characterization of fracture surface during dissolution. Geophysical Research Letters 30 (5), 1267, http://dx.doi.org/10.1029/2002GL016755.

Gunter, W.D., Perkins, E.H., Hitchon, B., 2000. Aquifer disposal of acid gases: modelling of water-rock reactions for trapping of acid wastes. Applied Geochemistry 15, 1085–1095.

Halim, C.E., Short, S.A., Scott, J.A., Amal, R., Low, G., 2005. Modeling the leaching of Pb, Cd, As, and Cr from cementitious waste using PHREEQC. Journal of Hazardous Materials 125, 45–61.

Hitchon, B., Gunter, W.D., Gentzis, T., Bailey, R.T., 1999. Sedimentary basins and greenhouse gases: a serendipitous association. Energy Conversion and Management 40, 825–843.

Huet, B.M., Prevost, J.H., Scherer, J.W., 2010. Quantitative reactive transport modeling of portland cement in CO_2-saturated water. International Journal of Greenhouse Gas Control 4, 561–574.

Houst, Y.F., 1992. Diffusion de gaz, carbonatation et retrait de la pate de ciment durcie. Thèse no. 1108, 1992, pp. 246.

Intergovernmental Panel on Climate Change (IPCC), 2005. In: Metz, B., Davidson, O., de Coninck, H.C., Loos, M., Mayer, L.A. (Eds.), Special Report on Carbon Dioxide Capture and Storage. Cambridge University Press, Cambridge, UK/NY, USA, pp. 195–276.

Jacquemet, N., Pironon, J., Caroli, E., 2005. A new experimental procedure for simulation of $H_2S + CO_2$ geological storage. Application to well cement aging. Oil and Gas Science and Technology 60, 193–206.

Kulik, D., Berner, U., Curti, E., 2004. Modelling Geochemical Equilibrium with the GEMS-PSI Code.

Kutchko, B.G., Strazisar, B.R., Huerta, N., Lowry, G.V., Dzombak, D.A., Thaulow, N., 2009. CO_2 reaction with hydrated class H well cement under geologic sequestration conditions: effects of flyash admixtures. Environmental Science and Technology 42, 6237–6242.

Kutchko, B.G., Strazisar, B.R., Dzombak, D.A., Lowry, G.V., Thaulow, N., 2007. Degradation of well cement by CO_2 under geologic sequestration conditions. Environmental Science and Technology 41, 4787–4792.

Lasaga, A.C., Kirkpatrick, R.J., 1981. Kinetics of Geochemical Processes, Rev. Mineral, vol. 8. Mineral. Soc. of Am., Washington, DC388.

Liteanu, E., Spiers, C.J., 2010. Fracture healing and transport properties of well-bore cement in the presence of supercritical CO_2. Chemical Geology 281, 195–210.

Lothenbach, B., Matschei, T., Moschner, G., Glasser, F.P., 2008. Thermodynamic modeling of the effect of temperature on the hydration and porosity of Portland cement. Cement and Concrete Research 38, 1–18.

Luquot, L., Gouze, P., 2009. Experimental determination of porosity and permeability changes induced by massive injection of CO_2 into carbonates reservoirs. Chemical Geology 265, 148–159.

Noiriel, C., Madé, B., Gouze, P., 2007. Impact of coating development on the hydraulic and transport properties in argillaceous limestone fracture. Water Resources Research 43, W09406, http://dx.doi.org/10.1029/2006WR005379.

Oldenburg, C.M., Bryant, S.L., Nicot, J.P., 2009. Certification framework based on effective trapping for geologic carbon sequestration. International Journal of Greenhouse Gas Control 3, 444–457.

Parkhurst, D.L., Appelo, C.A.J., 1999. User Guide to Phreeqc (version 2). A Computer Program For Speciation, Batch-Reaction, One-Dimensional Transport, 99-4259.326.

Plummer, L.N., Wigley, T.M.L., Parkurst, D.L., 1978. The kinetics of calcite dissolution in CO_2 water system at 5–60 °C and 0.0–1.0 atm CO_2. American Journal of Sciences 278, 179–216.

Regnault, O., Lagneau, V., Schneider, H., 2009. Experimental measurement of portlandite carbonation kinetics with supercritical CO_2. Chemical Geology 265, 113–121.

Rimmelé, G., Barlet-Gouédard, V., Porcherie, O., Goffe, B., Brunet, F., 2008. Heterogeneous porosity distribution in Portland cement exposed to CO_2-rich fluids. Cement and Concrete Research 38, 1038–1048.

Sauki, A.B., Irawan, S., 2010. Effect of pressure and temperature on well cement degradation by supercritical CO_2. International Journal of Engineering and Technology 10, 53–61.

Scherer, G.W., Celia, M.A., Prevost, J.-H., Bachu, S., Bruant, R., Duguid, A., Fuller, R., Gasda, S.E., Radonjic, M., Vichit-Vadakan, W., 2005. Leakage of CO_2 through abandoned wells: role of corrosion in cement. In: Benson, S.M. (Ed.), Carbon Dioxide Storage in Deep Geologic Formations—Results from the Carbon Capture. Project, vol. 2: Geologic Storage of Carbon Dioxide with Monitoring and Verification. Elsevier, London, UK, pp. 827–850.

Tai, C.Y., Chen, F.B., 1998. Polymorphism of $CaCO_3$ precipitated in a constant-composition environment. AIChE Journal 44 (8), 1790–1798.

Thiery, M., Villain, G., Dangla, P., Platret, P.G., 2007. Investigation of the carbonation front shape on cementitious materials: effects of the chemical kinetics. Cement and Concrete Research 37, 1047–1058.

Villain, G., Thiery, M., Platret, G., 2007. Measurement methods of carbonation profiles in concrete: thermo-gravimetry, chemical analysis and gamma-densimetry. Cement and Concrete Research 37, 1182–1192.

Wigand, M., Kaszuba, J.P., Carey, J.W., Hollis, W.K., 2009. Geochemical effects of CO_2 sequestration on fractured wellbore cement at the cement/caprock interface. Chemical Geology 265, 122–133.

Xu Tianfu, Apps, J.A., Pruess, K., 2004. Numerical simulation of CO_2 disposal by mineral trapping in deep aquifers. Applied Geochemistry 19, 917–936.